Measuring the subcellular compartmentalization of viral infections by protein complementation assay

Juliette Fernandez, Cédric Hassen-Khodja, Virginie Georget, Thierry Rose, Yves Jacob, Yves Louis Janin, Sébastien Nisole, Pierre-Olivier Vidalain, Nathalie J Arhel

Measuring the subcellular compartmentalization of viral infections by protein complementation assay

Juliette Fernandez[a], Cédric Hassen-Khodja[b], Virginie Georget[b], Thierry Rose[c], Yves Jacob[d], Yves L. Janin[e], Sébastien Nisole[a], Pierre-Olivier Vidalain[f,g], and Nathalie J. Arhel[a,1]

[a]Institut de Recherche en Infectiologie de Montpellier, CNRS, UMR 9004 Université de Montpellier, 34090 Montpellier, France; [b]Montpellier Ressources Imagerie, BioCampus Montpellier, CNRS, INSERM, Université de Montpellier, 34090 Montpellier, France; [c]Unité de Biologie Cellulaire des Lymphocytes, Institut Pasteur, INSERM 1221, 75015 Paris, France; [d]Unité de Génétique Moléculaire des Virus à Acide Ribonucléique, Institut Pasteur, CNRS UMR 3569, 75015 Paris, France; [e]Unité de Chimie et Biocatalyse, Institut Pasteur, CNRS UMR 3523, 75724 Paris, France; [f]Centre International de Recherche en Infectiologie, Université de Lyon, INSERM U1111, Université Claude Bernard Lyon 1, CNRS UMR 5308, École Normale Supérieure de Lyon, 69342 Lyon, France; and [g]Equipe Chimie et Biologie, Modélisation et Immunologie pour la Thérapie, Université Paris Descartes, CNRS UMR 8601, 75006 Paris, France

Edited by Stephen P. Goff, Columbia University Medical Center, New York, NY, and approved November 15, 2020 (received for review May 24, 2020)

The recent emergence and reemergence of viruses in the human population has highlighted the need to develop broader panels of therapeutic molecules. High-throughput screening assays opening access to untargeted steps of the viral replication cycle will provide powerful leverage to identify innovative antiviral molecules. We report here the development of an innovative protein complementation assay, termed αCentauri, to measure viral translocation between subcellular compartments. As a proof of concept, the Centauri fragment was either tethered to the nuclear pore complex or sequestered in the nucleus, while the complementary α fragment (<16 amino acids) was attached to the integrase proteins of infectious HIV-1. The translocation of viral ribonucleoproteins from the cytoplasm to the nuclear envelope or to the nucleoplasm efficiently reconstituted superfolder green fluorescent protein or NanoLuc αCentauri reporters. These fluorescence- or bioluminescence-based assays offer a robust readout of specific steps of viral infection in a multiwell format that is compatible for high-throughput screening and is validated by a short hairpin RNA-based prototype screen.

technological development | viruses | subcellular compartments

Infections by viruses represent a major burden for public health and a constant threat to humans. Despite critical needs, our therapeutic arsenal to fight viral infections is extremely limited and recent viral epidemics and pandemics have highlighted the need to develop innovative assays to allow for faster and better high-throughput primary screening aiming at the discovery of novel antiviral molecules. Phenotypic screening against whole viruses, rather than target-based screening, is a popular approach in the course of new viral emergence and pandemics since it does not require prior knowledge of the molecular target. Viral titration, RT-qPCR, or immunostaining and fluorescence imaging have been used extensively to measure viral replication. However, testing hundreds or thousands of conditions with these methods can be challenging. Alternatively, viral replication can be inferred from the measurement of virus cytopathic effects, but this readout is limited to lytic viruses (e.g., refs. 1 and 2). In addition, this method estimates viral replication only at the latest time point when the lysis of infected cells occurs. In another approach, recombinant viruses may be engineered to express reporter proteins, such as a fluorescent or bioluminescent molecule, from an additional transcription cassette or in frame with a viral coding sequence (e.g., refs. 3–5). However, some viral genomes or gene segments are relatively small and do not accommodate large insertions. Moreover, the use of reporter viruses relies on cellular transcription and translation machineries, which again implies later-time-point screening and the need to discriminate compound hits that target such cellular machineries.

To circumvent these limitations, we report here the development of an innovative protein complementation assay (PCA) to measure viral translocation between subcellular compartments. All viruses have evolved the mechanisms to traffic efficiently in their target cells to reach subcellular sites that sustain their replication and assembly (6, 7). For instance, influenza viruses, HIV, and most DNA viruses replicate their genome in the host cell nucleus. In our assay, termed αCentauri, a small fragment of a reporter protein named α (≤16 amino acids) is inserted in the viral genome to tag a relevant viral protein, while the complementary fragment named Centauri is tethered to a subcellular compartment (Fig. 1*A*). Viral translocation from the cytoplasm to that compartment reconstitutes the reporter and creates a gain of signal that can be measured by multiple readouts. As a proof of concept, a fluorescent (superfolder green fluorescent protein, sfGFP) (8) and a luminescent (NanoLuc, NLuc) (9) αCentauri reporter were adapted for PCA to precisely quantify two key steps of the HIV-1 replication cycle: the docking of viral ribonucleoproteins on the nuclear envelope and their entry into the nucleus (Fig. 1*B*).

The HIV particle comprises an envelope, a capsid, and two copies of positive-strand RNA genome. Following the fusion of the HIV envelope with the target cell membrane, the capsid is released into the cytoplasm and transported toward the nucleus. Reverse transcription of the genome into double-stranded DNA produces a preintegration complex (PIC), which enters the nucleus by active transport through the nuclear pore complex (NPC) and

Significance

The COVID-19 pandemic has highlighted the need to develop assays that can measure specific steps of viral replication on a large scale. Here we describe an innovative assay called αCentauri that uses fluorescence- or bioluminescence-based protein complementation assays to quantify the subcellular compartmentalization of viruses. As proof of concept, the Centauri fragment was tethered to the nuclear pore complex or sequestered in the nucleus, while the complementary α fragment was attached to the integrase proteins of infectious HIV-1. Thereupon the trafficking of HIV to the nucleus efficiently reconstituted superfolder green fluorescent protein and NanoLuc αCentauri reporters. This technology offers a robust readout of specific steps of viral infection in a multiwell format that is compatible for high-throughput screening.

Author contributions: J.F., T.R., Y.J., Y.L.J., S.N., P.-O.V., and N.J.A. designed research; J.F., V.G., and N.J.A. performed research; T.R., Y.J., Y.L.J., S.N., and P.-O.V. contributed new reagents/analytic tools; J.F., C.H.-K., V.G., and N.J.A. analyzed data; and N.J.A. wrote the paper.

Competing interest statement: J.F., S.N., and N.J.A. are inventors on a patent application describing the measurement of protein complementation upon nuclear import as described in this paper.

This article is a PNAS Direct Submission.

[1]To whom correspondence may be addressed. Email: nathalie.arhel@irim.cnrs.fr.

Published January 5, 2021.

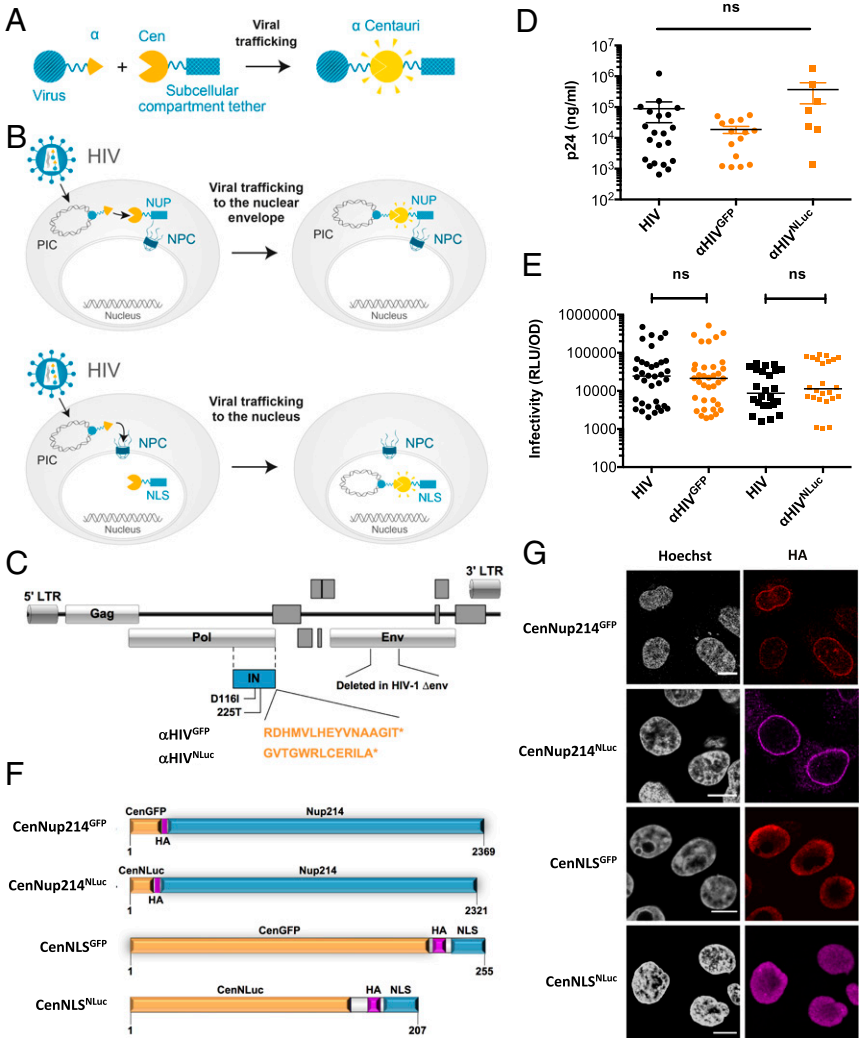

Fig. 1. Principle of the αCentauri assay and constructs. (*A*) Principle of the αCentauri PCA to monitor virus trafficking in infected cells. A fluorescent or luminescent reporter is split into two fragments of unequal size. The small α fragment is tagged to a relevant viral protein, while the larger Centauri (Cen) fragment is fused to a subcellular compartment tether. Upon viral trafficking, the α and Centauri fragments are brought into close proximity and assemble to form a functional αCentauri reporter. (*B*) αCentauri applied to monitor docking of HIV-1 at the nuclear envelope and entry into the nucleus. The small α fragment is tagged to HIV-1 IN, while the larger Centauri (Cen) fragment is fused either to Nup214 or to an NLS for targeting to the nuclear pore or to the nucleus, respectively. (*C*) Genomic organization of the HIV-1 constructs used in the study, indicating the insertion of α^{GFP} or α^{NLuc} in C-ter of viral IN. The genome is represented to scale using Illustrator for Biological Sequences. The 225T central polypurine tract (cPPT) mutant and D116I IN mutant are indicated. All experiments use Δenv VSV-G pseudotyped HIV-1 unless otherwise indicated. (*D*) Impact of the α insertion on virus production. HEK 293T cells were transiently transfected with full-length proviral expression plasmids (HIV, αHIV^{GFP}, or αHIV^{NLuc}). Virus production was measured by quantitation of p24 viral antigen in cell supernatants at 48 h posttransfection. Supernatants were either tested directly or after concentration by ultracentrifugation, therefore the resulting p24 concentrations ranged from ~10^3 to 10^6 ng/mL. Graphs show individual values from four independent experiments. Ordinary one-way ANOVA was performed using Prism 6; ns = nonsignificant ($P = 0.05$). (*E*) Impact of the α insertion on infectivity. Single-cycle virus titrations were carried out in P4 cells. β-galactosidase activity was measured by chemiluminescent assay at 48 hpi. Results are expressed as relative light units per second per nanogram of p24 of the inoculum, normalized for the optical density (OD) obtained by Bradford assay, mean SD of four independent experiments. Two-tailed paired *t* test was performed using Prism 6; ns = nonsignificant ($P = 0.56$ for αHIV^{GFP} and $P = 0.23$ for αHIV^{NLuc}). (*F*) Schematic representation of the Cen^{NLS} and Cen^{Nup214} constructs. Complementary fragments of the sfGFP (Cen^{GFP}) or Nanoluciferase (Cen^{NLuc}) were cloned upstream of a HA-tag followed by a SV40 NLS or the full-length sequence of Nup214. Amino acid positions are indicated below. (*G*) Localization of Cen^{NLS} and Cen^{Nup214}. Centauri constructs were exogenously expressed in HeLa cells by lentiviral transduction (NLS constructs) or plasmid transfection (Nup214). Localization was assessed by indirect HA immunolabeling at 48 h posttransduction or 24 h posttransfection. (Scale bars, 10 μm.)

mediates integration of the HIV DNA into the host cell chromatin (10, 11). Recent reports of intact HIV-1 capsids in the nucleus suggest that reverse transcription and uncoating can also occur after nuclear import near sites of integration (12, 13). In our assay, the αCen reporter is expressed as two complementary, self-assembling fragments of sfGFP or NLuc (14, 15). The small α fragment (α^{GFP}: 16 amino acids or α^{NLuc}: 13 amino acids) was fused into full-length and Δenv HIV-1 molecular clones (hereafter αHIV) in C-ter of HIV-1 integrase (IN) (Fig. 1*C*). Each incoming viral particle contains ~120 IN molecules bound to the RNA genome, based on the 20:1 synthesis ratio of Gag to Gag-Pol (16). After reverse transcription and shedding of the capsid, IN molecules that bind to the viral DNA ends as a multimer mediate integration (17), while free IN is inherently unstable and likely undergoes proteasomal degradation (18, 19). Insertion of the α-tag within the Pol coding sequence did not disrupt particle production (Fig. 1*D*) and ensured wild-type viral infectivity compared with nontagged viruses (Fig. 1*E*).

In parallel, the large fragment (Cen^{GFP}, 52 kDa or Cen^{Nluc}, 39 kDa) was fused to the nucleoporin Nup214 for targeting to the NPC (CenNup214) or to the triple nuclear localization signal

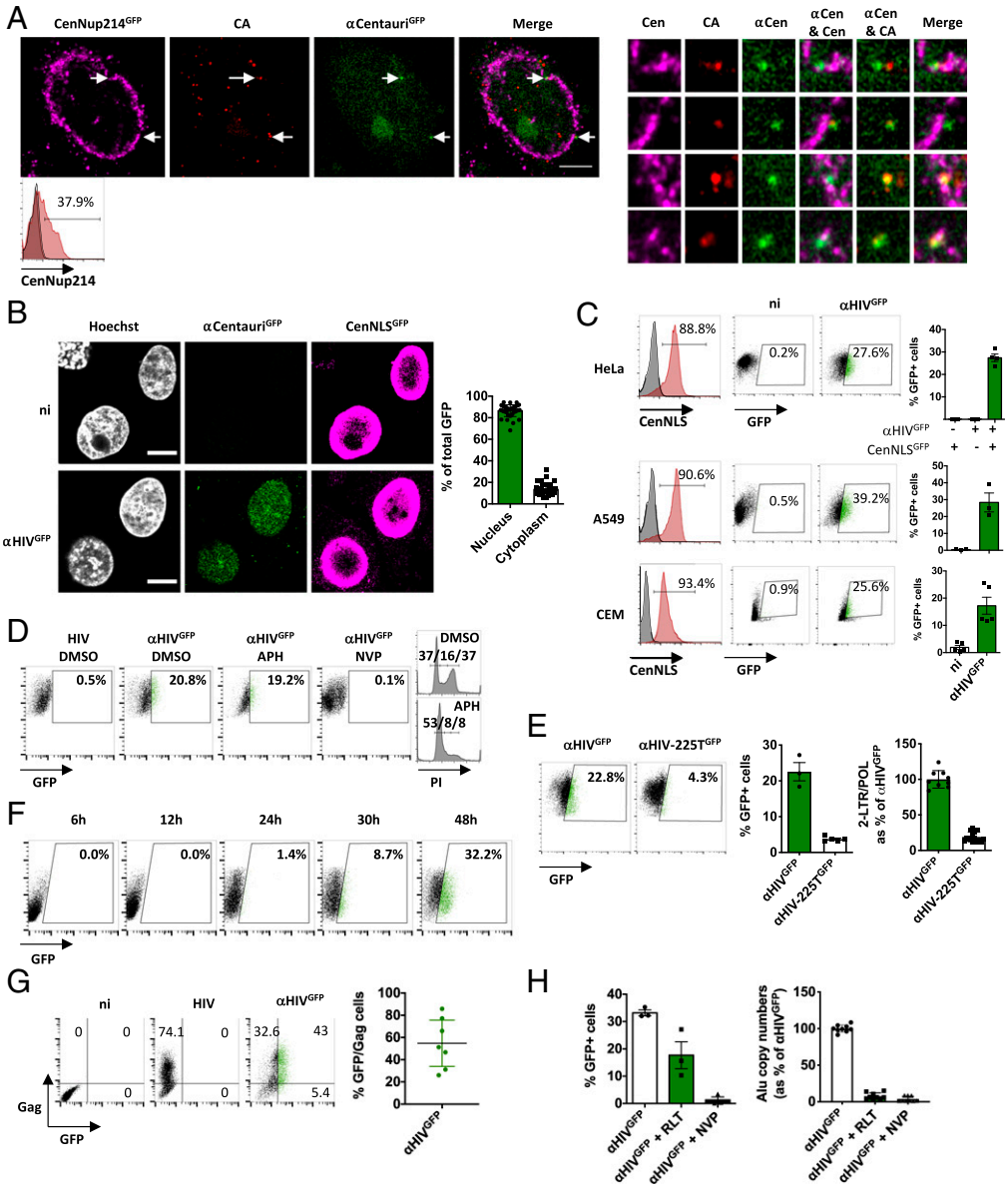

Fig. 2. Assessment of HIV-1 trafficking by fluorescent αCentauri^{GFP} assay. (*A*) HIV-1 trafficking to the nuclear pore generates αCentauri signal. HeLa cells transfected with CenNup214^{GFP} were infected with αHIV^{GFP} (VSV-G pseudotyped for all panels of Fig. 2) for 30 min. Images were acquired on an Airyscan LSM880 microscope. CenNup214^{GFP} was detected by HA labeling and HIV-1 capsid (CA) by labeling with AG3.0 monoclonal antibody. Arrows point to αCentauri^{GFP} spots, and insets show representative zoomed in images from two independent experiments. (Scale bar, 5 μm.) The flow cytometry plot shows CenNup214^{GFP} expression by HA labeling and is representative of three independent experiments. (*B*) HIV-1 trafficking to the nucleus generates αCentauri signal. HeLa cells transduced with CenNLS^{GFP} were infected with αHIV^{GFP}. αCentauri signal was imaged at 48 hpi using LSM700 confocal microscope. Images are representative from four independent experiments. Nuclear and cytoplasmic GFP signal was quantified using ImageJ on a total of 40 cells from seven independent fields. (Scale bars, 10 μm.) (*C*) αCentauri^{GFP} complementation in different cell types. Efficient transduction with CenNLS^{GFP} was assessed by indirect immunofluorescence labeling of the HA tag followed by flow cytometry (left histograms). Cells were then infected with αHIV^{GFP} or left uninfected (ni), and sfGFP signal was assessed by flow cytometry at 48 hpi (dot plots). Plots show representative experiments while graphs show individual values ± SEM from three independent experiments for each cell type. *D–H* are HeLa cells. (*D*) Effect of APH and NVP on αCentauri^{GFP}. CenNLS^{GFP} cells were treated with APH, NVP, or DMSO and infected with αHIV^{GFP}. GFP complementation was assessed at 48 hpi by flow cytometry. Cell cycle profiles were assessed by propidium iodide labeling (PI) (right histograms). Panels are representative of two independent experiments and numbers indicate the percentage of cells in G0-G1/S/G2-M phases of the cell cycle. (*E*) Assessment of a HIV-1 nuclear import mutant on αCentauri complementation. CenNLS^{GFP} cells were infected with αHIV^{GFP} or αHIV-225T^{GFP}. αCentauri complementation was measured at 48 hpi by flow cytometry. Plots are representative of three independent experiments, and the left-hand graph shows individual GFP values from three independent experiments with mean ± SEM. Viral nuclear import was assessed by qPCR quantification of 2-LTR circles normalized for late reverse transcripts (POL). The ratio of 2LTR/POL copy numbers was 0.01 to 0.5 for αHIV^{GFP} across experiments. Results are normalized for αHIV^{GFP}. The right-hand graph shows individual values from three independent experiments ± SD. (*F*) Time course of αCentauri^{GFP} complementation. CenNLS^{GFP} cells were infected with αHIV^{GFP} and fluorescent signal was measured at 6, 12, 24, 30, and 48 hpi. Results are representative of two independent experiments. (*G*) Frequency of αCentauri complementation in productively infected cells. CenNLS^{GFP} cells were infected with untagged HIV-1 or αHIV or left uninfected (ni). At 48 hpi, productive infection was assessed by indirect immunofluorescence labeling of intracellular Gag using KC67 antibody. Plots show one representative experiment, and the graph shows mean 95 CI for four independent experiments. (*H*) CenNLS^{GFP} cells were infected with αHIV either alone or in the presence of RTG or NVP. After 48 h, αCentauri complementation was assessed by flow cytometry. The graph shows the percentage of GFP+ cells from three independent experiments. HIV-1 integration was assessed by qPCR quantification of Alu-HIV segments. Results show individual values normalized for αHIV^{GFP} from three independent experiments performed in triplicate ± SD.

(NLS) of SV40 for tethering to the nucleus (CenNLS) (Fig. 1*F*). A hemagglutinin (HA) tag was introduced in all Cen constructs to monitor their expression and localization (Fig. 1*G*).

To assess αCentauri protein complementation following viral translocation from the cytoplasm to the nuclear envelope or to the nucleus, HeLa cells expressing CenNup214^{GFP} or CenNLS^{GFP} were infected with αHIV^{GFP}. Uninfected control cells did not emit any GFP fluorescence upon Centauri expression alone; however, infection by αHIV led to gain-of-GFP signal close to nuclear pores in CenNup214 cells (Fig. 2*A*) and in nuclei in CenNLS cells (with 87% of all GFP signal localizing to the nucleus) (Fig. 2*B*).

To further characterize αCentauri protein complementation following virus entry into the nucleus, several cell lines including T cells, which are the relevant target cells of HIV in vivo, were transduced with CenNLS and infected with αHIV. Complementation of sfGFP led to an ~5- to 10-fold increase in fluorescence in all tested cell types, while neither the α nor the Cen fragments emitted any detectable signal when expressed alone (Fig. 2*C*). To exclude that complementation occurred upon mixing of cytoplasmic and nuclear contents during cell division, aphidicolin (APH) was used as control to block nuclear envelope breakdown during mitosis. This treatment did not reduce signal, confirming that αCentauri signal is generated following viral transport through NPCs, which is concordant with the HIV PIC entering the nucleus through nuclear pores (Fig. 2*D*). Next, we showed that treatment of cells with nevirapine (NVP), a reverse transcription inhibitor that delays uncoating (13, 20–22), prevented αCentauri complementation at 48 h postinfection (hpi), suggesting that only productive infection events generate signal (Fig. 2*D*). In addition, nuclear PCA was inhibited following infection with a HIV-1 mutant that is defective for nuclear entry [225T (23)], confirming that viral nuclear import is both necessary and sufficient for CenNLS complementation (Fig. 2*E*). Of note, although signal was detectable as of 24 hpi, complementation was optimal at 48 hpi (Fig. 2*F*). This comes substantially later than entry of HIV-1 into the nucleus, which is believed to occur within 8 hpi (12, 13). Moreover, indirect immunofluorescence detection of Gag indicated that only ~60% productively infected cells were αCentauri-positive (Fig. 2*G*). The delay between nuclear import and fluorescent signal reflects the previously reported kinetics for the appearance of fluorescence following bimolecular complementation, which allow for assembly and maturation and can last up to 20 h (24). Since αCentauri measurements were performed several hours after viral nuclear import, it was possible that PCA also occurred following nuclear entry of neosynthesized α-tagged IN. HIV-1 Gag and Gag-Pol polyproteins have been shown to traffic back to the nucleus and perinuclear area after translation in the cytoplasm (25). As a control, we therefore performed infections in the presence of an integrase inhibitor (raltegravir, RTG) to prevent de novo synthesis of viral proteins. Although signal was decreased by approximately twofold in the presence of RTG, the levels of reconstituted sfGFP remained 1 to 2 log above the NVP control, thus confirming that our assay provides a reliable readout of viral nuclear import (Fig. 2*H*).

To overcome the low sensitivity and slow assembly kinetics of the fluorescent reporter, we adapted αCentauri to a luminescence reporter, since this reporter system exhibits a wide dynamic range with a high sensitivity and virtually no background (9). Complementation of NLuc following infection of CenNLS^{NLuc} cells with αHIV^{NLuc} was measured by plate luminometry. In this system, the αCentauri complementation reporter was less bright (1 to 3 log) than native NLuc, because of the reduced stability of the reporter fragments (15). Moreover, luminescent signal is dependent on the intrinsic affinity and propensity to self-associate in a defined compartment, and on the probability of a virus docking at the nuclear pore, or entering the nucleus, which is less likely than classical protein-fragment complementation. Still, infection resulted in 5- to 200-fold increase in emitted luminescence signal in all tested cell types, including T cells (Fig. 3*A*). The luminescence signal was proportional to CenNLS expression level as illustrated in HeLa cells (Fig. 3*B*). Signal was detected as early as 16 hpi and was optimal at 24 hpi (Fig. 3*C*) and was also detectable following infection with wild-type envelope HIV (Fig. 3*D*). Moreover, the αCentauri signal intensity was directly proportional to the detection of the HIV-1 genome in the nucleus, confirming that the NLuc reporter was reconstituted upon HIV-1 PIC nuclear import (Fig. 3*E*).

We therefore introduced a D116I mutation in viruses to block integration and all downstream steps of viral replication. Infection with D116I virus still achieved *ca*. 10-fold increase in NLuc compared to infection in the presence of NVP (Fig. 3*F*), confirming that αCentauri allows the detection of genuine viral PICs translocating from the cytoplasm into the nucleus.

In principle, the αCentauriNLS assay reflects the combined efficiency of all the early steps of viral replication required to reach the nucleus and is not specific to nuclear import. However, we reasoned that by performing αCentauriNup214 and αCentauriNLS side by side in the context of a single high screening platform the system would allow deconvoluting successful trafficking to the NPC from HIV nuclear import and therefore enable the specific screening of nuclear import. Since the sfGFP approach was poorly quantitative for Nup214, we tested the NLuc readout. To assess αCentauri protein complementation following virus docking at the nuclear envelope, HeLa cells were transduced or transfected with CenNup214 then infected with αHIV. Infection resulted in a 10-fold increase in signal, indicating that the αCentauriNup214 assay is quantitative and could be used in parallel to αCentauriNLS to screen for specific inhibitors of nuclear import (Fig. 3*G*).

Currently, the paramount screening strategy for HIV replication relies on the HIV long-terminal repeat promoter (LTR) whose transcriptional activity is turned on by the early HIV gene product Tat. LTR-reporter cell lines, using LacZ, enhanced GFP (EGFP), or luciferase, have been used in the past to identify cellular cofactors of HIV infection (26, 27). Alternatively, infected cells can be scored by immunolabeling of viral antigens. We have therefore compared αCentauri^{GFP} and αCentauri^{NLuc} assays with an LTR-LacZ system and with the labeling of intracellular Gag (iGag) to score HIV-infected cells. Results revealed that the αCentauri^{NLuc} system exhibits a wide dynamic range with a maximum/minimum ratio of 65, compared with 19 for the LTR-LacZ system and <3 for αCentauri^{GFP} and iGag (Fig. 4*A*). The assay also exhibited high sensitivity, virtually no background, and a linear dose–response over 2 log, which was superior to any other tested assay (Fig. 4*A*).

This assay initially used the commercially available Nano-Glo bioluminescence-based reporting system which is made of the NanoLuc/NanoKAZ luciferase and uses furimazine as its substrate (9, 28). In an attempt to improve its sensitivity, we also evaluated a series of coelenterazine analogs including furimazine (Z01) that were previously characterized as NanoLuc substrates (29, 30). Accordingly, the corresponding *O*-acetylated proluciferins (hikarazines 01, 03, 97, 103, and 108) were hydrolyzed and the resulting solutions of these luciferin analogs assessed at a final concentration of 40 to 50 μM. As compared with the Nano-Glo kit, which was used according to the manufacturer's instructions, all these luciferin analogs actually led to a greater signal intensity. Even hikarazine-1 (Z01), which yields furimazine, provided a slightly improved bioluminescence signal. Particularly noteworthy are the luciferin solutions obtained from Z03, Z97, and Z108 which gave the highest relative light unit values following infection with αHIV^{NLuc}, with respective signals 6-, 11-, and 11-fold higher than the ones observed with Nano-Glo (Fig. 4*B*). The best discrimination between positive and negative samples was obtained with Z03 (30-fold), Nano-Glo (20-fold),

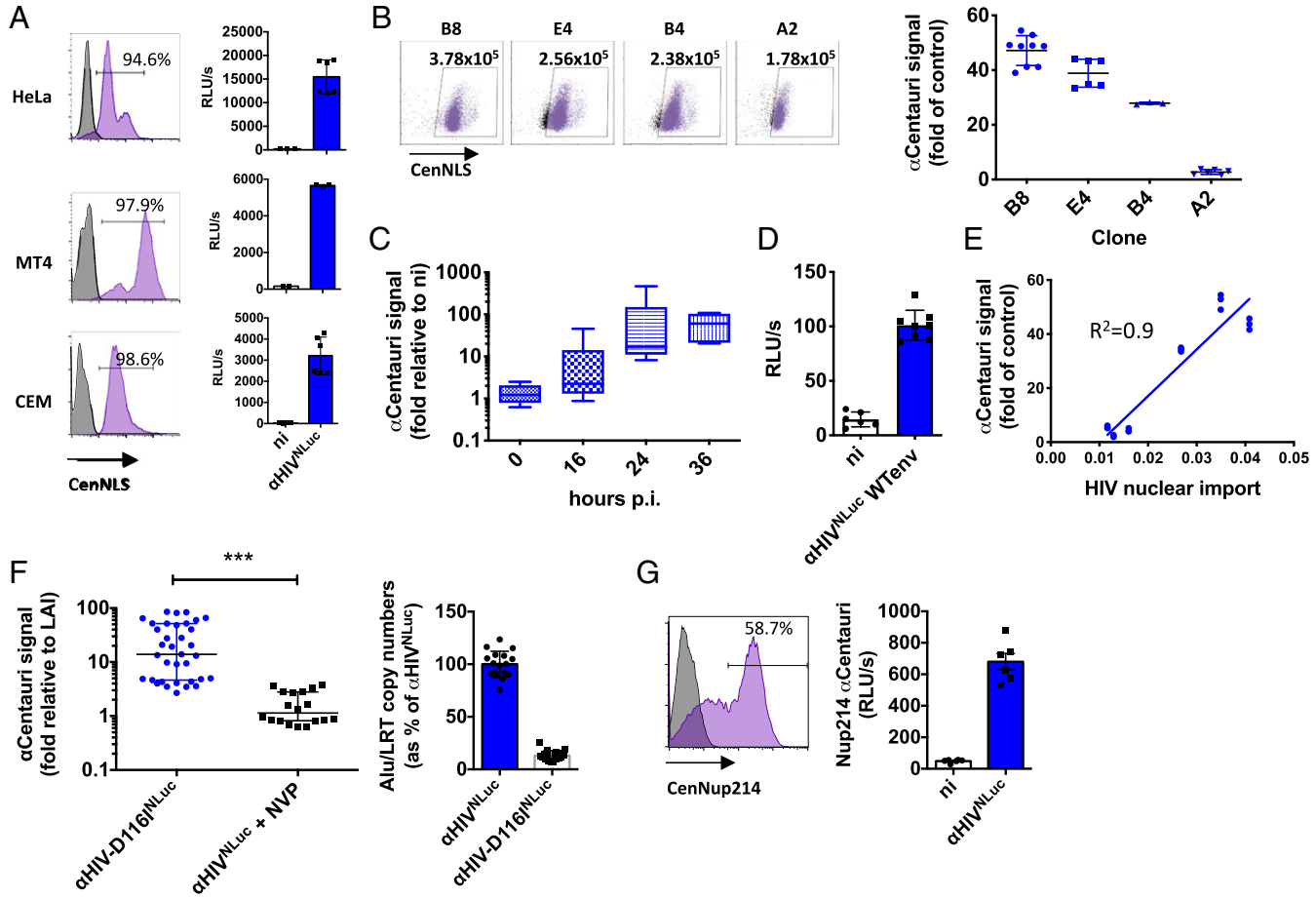

Fig. 3. Assessment of HIV-1 trafficking by luminescent αCentauri^{NLuc} assay. (*A*) αCentauri^{NLuc} complementation in different cell types. Efficient transduction with CenNLS^{NLuc} was assessed by indirect immunofluorescence labeling of the HA tag followed by flow cytometry (left histograms). Cells were then infected with αHIV^{NLuc} or left uninfected (ni), and NLuc signal was assessed as relative light units per second by plate luminometry at 24 hpi. Graphs show individual values ± SEM from two independent experiments. All subsequent panels are HeLa cells unless otherwise stated. (*B*) αCentauri^{NLuc} signal is related to the efficiency of Cen^{NLuc} expression. CenNLS^{NLuc} cell clones were characterized by HA-labeling. Cytometry plots are representative of four independent labeling experiments. The measurement of transduction efficiency is provided as the product of the geometric mean fluorescence and percentage HA+ cells. Clones were then infected with αHIV^{NLuc} or with untagged HIV-1 (control), and NLuc complementation was assessed after 24 h and normalized for protein content by Bradford assay. The graph shows individual values and mean ± SD from two independent experiments. (*C*) Time course of αCentauri^{NLuc} complementation. CenNLS^{NLuc} cells were infected with αHIV^{NLuc} and luminescent signal was measured at 16, 24, and 36 hpi and represented as fold signal (relative light units per second) above uninfected background control. Results show all values from three independent experiments as box and whisker plots. (*D*) αCentauri assay using wild-type envelope HIV-1. CenNLS^{NLuc} P4 cells were infected with αHIV^{NLuc} (WTenv) and luminescent signal was measured at 24 hpi. Results show relative light units per second values from two independent experiments. (*E*) αCentauri complementation in the nucleus correlates with HIV-1 genome nuclear import. CenNLS^{NLuc} cells were infected with different doses of αHIV^{NLuc}. Viral nuclear import was assessed by qPCR quantification by the ratio of 2-LTR circles over total reverse transcribed HIV (POL). αCentauri was measured at 24 hpi for each condition and normalized for protein content by Bradford assay. The graph shows individual values relative to untagged HIV-1 control from three independent CenNLS^{NLuc} clones. (*F*) Integration-defective HIV-1 generates robust αCentauri complementation. CenNLS^{NLuc} cells were infected with two POL copies per cell of αHIV, αHIV with NVP, αHIV-D116I^{NLuc}, or untagged HIV-1 for 24 h. The left graph shows individual values (as fold increase in relative light units per second relative to untagged HIV-1) from three independent experiments performed on a total of 12 Cen^{NLuc} HeLa cell lines and median with interquartile range. Statistical analysis was performed by unpaired *t* test using Prism 6. ***$P = 0.0002$. HIV-1 integration was assessed by qPCR quantification of Alu-HIV segments and reverse transcribed HIV (late reverse transcripts). Results are normalized for αHIV^{NLuc}. The right-hand graph shows individual values from three independent CenNLS^{NLuc} clones ± SD. (*G*) αCentauri^{NLuc} allows quantification of HIV-1 docking at nuclear pores. HEK 293T cells were transfected with CenNup214 by calcium phosphate coprecipitation then seeded in 96-well plate and infected with αHIVNLuc. NLuc signal was detected at 6 hpi. Results show independent values from two independent experiments.

Z97 (17-fold), and Z01 (10-fold) (Fig. 4*B*). The lowest ratio between αHIV^{NLuc} over αHIV^{NLuc} + NVP was obtained with Z103 (fivefold). Therefore, we suggest that the *O*-acetylated coelenterazine analogs hikarazine-03 (Z03) and hikarazine-97 (Z97), which lead to the corresponding luciferins upon hydrolysis, are particularly suited for performing αCentauri^{NLuc} screens.

In order to validate our assay for screening, we also assessed plate uniformity and minimum-to-maximum discrimination by performing assays in 96-well format. Plates were laid out in interleaved format by alternating positive and negative controls. This enabled us to calculate the Z′ factor, an indicator of the quality of a screening assay. Both αCentauri^{GFP} and αCentauri^{NLuc} presented good discrimination between positive and negative controls with Z′ of 0.63 for αHIV^{GFP}, 0.74 for αHIV^{NLuc}, and 0.35 for αHIV-D116I^{NLuc} compared with the NVP negative control (Fig. 4*C*). Signal/background ratios were 2.53 for αHIV^{GFP} and 30.26 and 5.07 for αHIV^{NLuc} and αHIV-D116I^{NLuc}, respectively, which was considered acceptable since >2. Signal/noise ratios were 34.32 for αHIV^{GFP} and 280.77 and 39.07 for αHIV^{NLuc} and αHIV-D116I^{NLuc}, respectively, which was considered acceptable since >10.

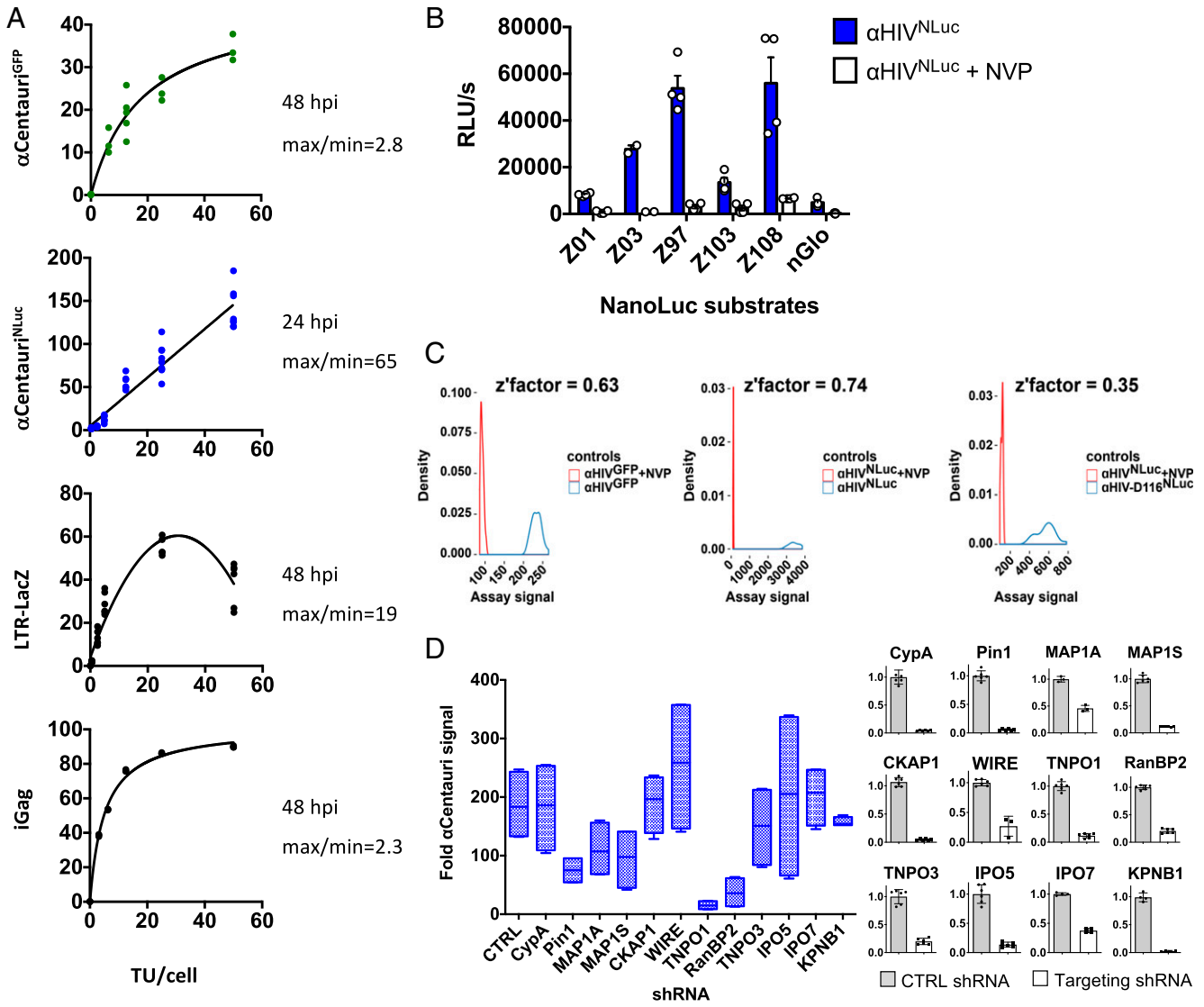

Fig. 4. Benchmarking and quality control of αCentauri toward screening. (*A*) Comparison of αCentauri with alternative assays of HIV-1 replication used for screening. Four HIV infection reporter systems were tested for readout at different TU per cell. (*Top*) HeLa cells were transduced with CenNLS^{GFP} then infected with αHIV^{GFP} at the indicated TU per cell. The graph plots the percentage of GFP-positive cells at 48 hpi assessed by flow cytometry and shows individual values from four independent experiments with a hyperbola curve fit (R^2 = 0.93). (*Upper Middle*) HeLa-CenNLS^{NLuc} cells were infected with αHIV^{NLuc} at the indicated TU per cell. The graph plots the relative increase in relative light units per second at 24 hpi (as fold relative to untagged HIV-1) and shows individual values from four independent experiments with a linear regression (R^2 = 0.91). (*Lower Middle*) HeLa-LTR-LacZ cells were infected with HIV-1 at the indicated TU per cell. The β-galactosidase signal was measured at 48 hpi using a chemiluminescent assay kit from Roche according to manufacturer's instructions and normalized for protein content measured by Bradford assay. Individual values × 10^2 from two independent experiments are shown with a second-order polynomial fit (R^2 = 0.89). (*Bottom*) HeLa cells were infected with HIV-1 at the indicated TU per mL. At 48 hpi, cells were fixed and labeled with an anti-gag KC67 antibody to assess the percentage of infected cells by flow cytometry. The graph shows a single representative experiment with a hyperbola curve fit (R^2 = 0.99). For each graph, minimum/maximum values show the fold signal between the highest and lowest infectious dose for each assay. (*B*) Comparison of different fumirazine substrates with commercial Nano-Glo (nGlo). CenNLS^{NLuc} HeLa cells were infected with αHIV. At 24 hpi, substrate was added directly to each well with a 1:1 ratio. Luminescence was measured 3 min after substrate addition. Final substrate concentration was 40 to 50 μM, except for Nano-Glo where the stock concentration was not provided by the manufacturer (Promega). The graph shows individual values from two independent experiments. (*C*) Quality control distribution of positive and negative controls. Z′ factors were calculated for αCentauri^{GFP} using αHIV^{GFP} versus αHIV^{GFP} with NVP, and for αCentauri^{NLuc} using αHIV^{NLuc} or αHIV-D116I^{NLuc} versus αHIV^{NLuc} + NVP. Examples are representative of three independent experiments. (*D*) shRNA-based screen of cellular cofactors of HIV-1 nuclear import using αCentauri. HeLa CenNLS$_{NLuc}$ stable clones were transduced with lentiviral vectors coding for the indicated shRNAs for 2 d then infected with αHIV^{NLuc} or untagged HIV-1 at 50 Pol copies per 20,000 cells and αCentauri signal was measured at 24 hpi using NanoGlo substrate. NLuc signal (relative light units per second) was normalized for protein content in each well by Bradford assay, and values for αHIV^{NLuc} were normalized as fold values over background values obtained with untagged HIV-1. The graph shows a box and whisker plot of two independent experiments performed in duplicate. Right-hand graphs show levels of knockdown obtained by qPCR analysis of the indicated transcripts, as individual values from experimental replicates and mean ± SD.

Finally, to achieve a proof of concept, we performed a short hairpin RNA (shRNA)-based screen that included proteins known to mediate HIV-1 nuclear import, as well as related proteins previously shown to have little effect on HIV-1. Among proteins known to promote HIV entry in the nucleus, MAP1A and MAP1S contribute to retrograde trafficking (31), RanBP2 anchors capsids at the NPC (32–34), TRN-1/TNPO1 triggers productive uncoating (35), and TNPO3 indirectly regulates

capsid stability via its cargo CPSF6 (26, 36, 37). Among proteins that were not expected to have much effect on entry of the viral genome in the nucleus, CypA has no effect in HeLa cells (38, 39), KPNB1 mediates Tat nuclear import independently of PIC entry (35, 40), and β-karyopherins IPO5 and IPO7 (35) and cytoskeletal proteins CKAP1 and WIRE (31) have a low to moderate effect on infection. HeLa-CenNLS^{NLuc} cells were treated with previously validated shRNAs against these cellular cofactors, infected with αHIV^{NLuc}, and NLuc signal was measured at 24 hpi. The knockdown of RanBP2 and TRN-1/TNPO1 had the greatest effect on HIV nuclear import, leading to a ∼10-fold decrease in αCentauri. Other proteins that came out as relevant cofactors were Pin1, MAP1A, and MAP1S, thus confirming previous findings (31, 41). Conversely, shRNAs against CKAP1, TNPO3, IPO5, IPO7, and KPNB1 led to marginal reduction in αCentauri signal (Fig. 4*D*). Although this result confirms our previous work demonstrating an important role for TNPO1 in HIV-1 uncoating and nuclear import (35), it is seemingly at odds with previous findings showing comparatively more effect with shRNAs against TNPO3 than TNPO1 (42, 43). However, since shRNAs against TNPO3 may impact HIV-1 predominantly after its nuclear import (44–46), this will likely undermine their effect on the signal generated by reporter complementation in the nucleus. Taken together, results confirm that αCentauri is a quantitative and reliable assay, applicable to the screening of shRNA/CRISPR-Cas9 libraries or small compound libraries (47).

Discussion

The recent emergence and reemergence of viruses in the human population has highlighted the need for cell-based assays of viral replication. The measure of viral cytopathic effects or the detection of viral proteins by antibody labeling or insertion of fluorescent reporter genes are standard approaches for primary screening before target identification. However, they are not applicable to all viruses and suffer from significant drawbacks such as high cost, poor quantitative readout, and disruption of virus properties. Here we report the development of a highly quantitative readout of viral replication based on the quantification of viral translocation between subcellular compartments by proximity-based PCA. As proof of concept, we applied αCentauri to the detection of HIV translocation to nuclear pores and to the nucleus. Since all viruses traffic between different subcellular compartments to replicate, including between the plasma membrane, endocytic vesicles, the cytoplasm, the nucleus, and endoplasmic reticulum, we believe that this assay is applicable to any virus.

The overarching advantage of using proximity-based PCA for screening is that the readout is independent of the cellular transcription and translation machineries. This provides a cleaner readout since compounds that indiscriminately affect these machineries (DNA intercalators, histone modifiers, cell cycle inhibitors, etc.) will not be scored as hits. Such split-reporter assays or specialized enzymatic fusion assays have previously been applied to monitor viral infection in cells, but these all rely on the indiscriminate expression of the complementary reporter fragment or enzyme substrate throughout the target cell (48–50). As a result, these assays only provide a readout of cell entry and would not flag potent antivirals that act at later stages. Here the originality of our approach is to tether Centauri to a subcellular compartment to monitor viral trafficking between compartments. A successful translocation brings together two reporter fragments that do not emit any signal alone, creating a binary gain of signal, unlike the use of fluorescent fusion proteins whose colocalization with subcellular compartments tends to be more qualitative than quantitative. Additionally, the approach allows us to quantify a specific step of viral replication, whereas assays that rely on a reporter or lytic activity measure the entire replicative cycle.

Both split reporter systems (sfGFP and NLuc) were chosen because they have the smallest α tag, allowing viral functions to be preserved. The two methods offer complementary advantages with limited drawbacks. Split GFP has the advantage that the PCA interaction is indissociable (14), which means the signal remains stable for some time and allows the measurement of cumulated nuclear import events. The signal can be visualized by fluorescent microscopy or analyzed by flow cytometry without any other special treatment of the cells. Moreover, αCentauri^{GFP} is compatible with high-content screening, allowing correlating GFP signal with HA and Gag signal, precisely pinpointing the site of complementation, with shRNA transduction efficiency, and with Hoechst labeling of nuclei to normalize results and exclude toxic compounds. The NanoLuc readout is more adapted to high-throughput screening since it offers signal linearity over 2 log (Fig. 4*A*). NLuc expression is transient and is thought to be dissociable, making it more adapted to dynamic assays. Moreover, the luminescent NLuc reporter offered earlier readout, higher amplitude, greater sensitivity, and lower background and a better discrimination between positive and negative controls. It also offered a linear assay over a wide range of multiplicity of infection (MOI).

In the case of the HIV, there is today no clear understanding of how the PIC passes through the NPC into the nucleus. Currently, the only available methods to quantify HIV nuclear import rely either on the imaging of virus components in the nucleus (for instance refs. 51–53) or on the measurement of unintegrated viral DNA that forms only in the nucleus (54). However, viral protein and unintegrated DNA are extremely sparse in the nucleus, and their detection fluctuates with time, making these assays incompatible with high-throughput screening (36, 55, 56). αCentauri applied to HIV trafficking provides an approach to study nuclear import, to identify key cofactors and potential inhibitors.

Methods

Cells and Drugs. P4 TAR-β-gal indicator cells are HeLa CD4+ CXCR4+ CCR5+ carrying the LacZ gene under the control of the HIV-1 LTR promoter (AIDS Reagent Program). HEK 293T (CRL-11268), HeLa (CCL-2), and A549 (CCL-185) were obtained from the ATCC and were cultured in Dulbecco's modified Eagle's medium-GlutaMAX supplemented with 10% fetal calf serum (FCS) and penicillin/streptomycin (all Gibco by Life Technologies). The MT4R5 (57) and CEM CD4+ (AIDS Reagent Program) T cell lines were grown in RPMI medium with 10% FCS, 100 IU/mL penicillin, and 100 μg/mL streptomycin. NVP (Sigma) was used at a working concentration of 5 μM for the duration of the experiment. APH (Sigma) was added to cells at the concentration of 8 μM for 24 h before infection and maintained for the duration of the experiment.

αCentauri Sequences. Amino acid sequences of sfGFP and NanoLuc, indicating the site of the split as a vertical line, are as follows:

sfGFP (Cen^{GFP} in regular font, αGFP in bold) (based on ref. 14):

MVSKGEELFTGVVPILVELDGDVNGHKFSVRGEGEGDATIGKLTLKFICTTGKLPV-PWPTLVTTLTYGVQCFSRYPDHMKRHDFFKSAMPEGYVQERTISFKDDGKYKT-RAVVKFEGDTLVNRIELKGTDFKEDGNILGHKLEYNFNSHNVYITANKQKNGIKA-NFTVRHNVEDGSVQLADHYQQNTPIGDGPVLLPDNHYLSTQTVLSKDPNEK|**RDH-MVLHEYVNAAGIT**

NanoLuc (Cen^{NLuc} in regular font, αNluc in bold) (based on ref. 15):

MVFTLEDFVGDWEQTAAYNLDQVLEQGGVSSLLQNLAVSVTPIQRIVRSGENALK-IDIHVIIPYEGLSADQMAQIEEVFKVVYPVDDHHFKVILPYGTLVIDGVTPNMLNYF-GRPYEGIAVFDGKKITVTGTLWNGNKIIDERLITPDGSMLFRVTIN|**GVTGWRLCER-ILA**

Construction and Production of αCentauri Viruses and Vectors. All viruses were HIV-1 LAI, either full-length or Δenv and pseudotyped with the vesicular stomatitis virus glycoprotein (VSV-G). αHIV^{GFP}, αHIV-225T^{GFP}, or αHIV^{Nluc} viral constructs were generated by PCR using a pBlueScript (pBS) plasmid containing a PstI-NcoI fragment of the HIV-1 LAI wild-type or mutant 225T

Table 1. Primers and probes used for the qPCR experiments

PCR	Primer name	Sequence (5′–3′)
LRT	MH531	TGTGTGCCCGTCTGTTGTGT
	MH532	GAGTCCTGCGTCGAGAGAGC
	LRT-P	(FAM)-CAGTGGCGCCCGAACAGGGA-(TAMRA)
2-LTR	MH535	AACTAGGGAACCCACTGCTTAAG
	MH536	TCCACAGATCAAGGATATCTTGTC
	MH603	(FAM)-ACACTACTTGAAGCACTCAAGGCAAGCTTT-(TAMRA)
β actine	β actin fwd	aacaccccagccatgtacgt
	β actin rev	cggtgaggatcttcatgaggtagt
	β actin probe	(FAM)-ccagccaggtccagacgcagga-(BBQ)
Alu-PCR	MH535	AACTAGGGAACCCACTGCTTAAG
	SB704	TGCTGGGATTACAGGCGTGAG
	MH603	(FAM)-ACACTACTTGAAGCACTCAAGGCAAGCTTT-(TAMRA)
	L-M667 modified	atgccacgtaagcgaaactttccgctggggactttccaggg
	Alu 1	TCCCAGCTACTGGGGAGGCTGAGG
	Alu 2	GCCTCCCAAAGTGCTGGGATTACAG
	Lambda T	ATGCCACGTAAGCGAAACT
	U5-specific primer	ctgactaaaagggtctgagg
	nested probe	(FAM)-ttaagcctcaataaagcttgccttgagtgc-(TAMRA)
POL	pol fwd	TTTAGATGGAATAGATAAGGCCCAA
	pol rev	CAGCTGGCTAACTATTTCTTTTGCTA
	pol probe	(FAM)-AATCACTAGCCATTGCTCTCCAATTAC-(TAMRA)
RPL13A	RPL13A-Fq	AACAGCTCATGAGGCTACGG
	RPL13A-Rq	TGGGTCTTGAGGACCTCTGT
Pin1	Pin1-Fq	GAGAAGATCACCCGGACCAA
	Pin1-Rq	AAAGTCCTCCTCTCCCGACT
CypA	CypA-Fq	GCCGAGGAAAACCGTGTACT
	CypA-Rq	GTCTGCAAACAGCTCAAAGGAG
TRN-1	TRN-1-Fq	TTCGAATGGATCGCCTGCTT
	TRN-1-Rq	CCGTCCTCGATCGGTGAAAA
TNPO3	TNPO3-Fq	CAGCTGGAACCAGACCATGA
	TNPO3-Rq	CAGCTGGAACCAGACCATGA
IPO5	IPO5-Fq	TTGCGTCCTCACTTGGAAGC
	IPO5-Rq	AAGTCCGCAAGCCATTCGAT
IPO7	IPO7-Fq	CAGAGGAGCGGAGTCCATTG
	IPO7-Rq	CCCACTTCTTGCATTTCCACC
MAP 1A	MAP 1A-Fq	CTTCCCGGAGGTTTGAGGAC
	MAP 1A-Rq	AGAGAGGCTTCGGTCAGGAT
MAP 1S	MAP 1S-Fq	TCCTGGAGGAGCTCGAAAGA
	MAP 1S-Rq	GGAGAAGGTGGCAGAGTGTC
CKAP1	CKAP1-Fq	CCTCACCATCGCTGAGTTCAA
	CKAP1-Rq	TCCAGCTTGCTGTAGAACTTGT
WIRE	WIRE-Fq	GCGCCCTCTTACAGGACATT
	WIRE-Rq	CTTCTCGAGGATGGGAGCAC
RanBP2	BP2-Fq	ACAATGGAATTAAAGCCCTTAAATGT
	BP2-Rq	GAAACAATCAGCTACTTCTTTAGTTTTA
KPNB1	KPNB1-Fq	GTCACAAACCCCAACAGCAC
	KPNB1-Rq	AGCCACTCGTACCCTCGTAT

molecular clone. Briefly, oligonucleotides coding for αGFP or αNluc flanked by EcoRI and NdeI restriction sites were used to amplify and add αGFP or αNluc in C-ter of HIV-1 integrase. The forward primer was 5′-CCAGTACTACGGTTAAGGC-3′. Reverse primers were αGFP 5′-GAAACATACATATGCTATGTAATCCCAGCAGCATTTACGTACTCATGAAGGACCATGTGGTCACGAGCGGCCGCATCCTCATCCTGTCTACTTG-3′ and αNluc 5′-GAAACATACATATGTTACGCCAGAATGCGTTCGCACAGCCGCCAGCCGGTCACTCCGTGGTCACGAGCGGCCGCATCCTCATCCTGTCTACTTG-3′. PCR products were digested with EcoRI/NdeI and cloned into pBS-LAI (PstI-NcoI). Finally, the PstI-NcoI fragment of LAI containing IN fused to αGFP or αNluc was cloned back into a wild-type Env or ΔEnv HIV-1 LAI molecular clone. αHIV-D116I^{Nluc} was obtained by site-directed mutagenesis using the QuikChange II site-directed mutagenesis kit (Agilent) on the pBS-LAI containing IN fused to αNluc and was then cloned back into a wild-type Env or ΔEnv HIV-1 LAI molecular clones.

Lentiviral vectors (LV) coding for CenNLS or CenNup214 were obtained by cloning HA-NLS or HA-Nup214 downstream of Cen^{GFP} or Cen^{Nluc} by PCR amplification. Cen^{GFP}NLS was generated by strand-overlap PCR first by generating Cen^{GFP}-HA from a GFP1-10 plasmid (14) using the following primers: 5′- GATCGGATCCCGCCACCATG and 5′- AAGAGCGTAATCTGGAACATC GTATGGGTAGCCGGCGCCTTTCTCGTTTGGGTCTTTGCTCAGC-3′. Then, GFP-HA-NLS was generated by a second PCR and cloned into an HIV-1–derived vector with BamH1/XhoI restriction enzymes. Cen^{NLuc}NLS was synthesized by Genscript and cloned into a pcDNA3.1(+), followed by an HIV-1–derived vector. CenNup214 constructs were generated by amplifying Cen^{GFP}-HA or Cen^{NLuc}-HA with AgeI and NotI overhangs and subcloning these at the place of EGFP upstream of Nup214 using a pEGFP-Nup214 plasmid (Euroscarf).

All viruses and vectors were produced by transient transfection of HEK 293T cells by calcium phosphate precipitation with the proviral or LV plasmid, cotransfected with VSV-G expression plasmid for Δenv viruses and vectors, and with an encapsidation plasmid (pCMVΔR 8.74) for vectors. Viruses and vectors were harvested at 48 h after transfection. Viruses were concentrated using Lenti-X Concentrator (Clontech) and vectors by ultracentrifugation for 1 h at 64,000 × *g* (Beckman Coulter) at 4 °C.

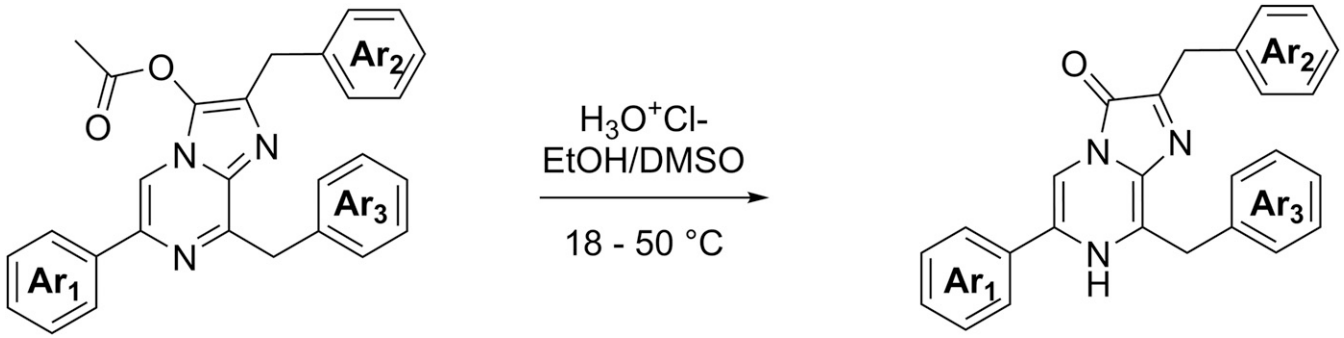

Scheme 1. Generation of luciferin solutions from *O*-acetylated luciferin.

Centauri Expression. Cells were transduced with CenNLS^{GFP} and CenNLS^{NLuc} at MOI 10. Cells were used at 48 h posttransduction , or stable cell lines were generated by selection and expansion of clones using neomycin (1 mg/mL). Cells were transfected with CenNup214^{GFP} and CenNup214^{NLuc} plasmids using Fugene6 (Roche, HeLa) or calcium phosphate precipitation (HEK 293T) using 2 μg per 10^6 cells. The efficiency of transduction and transfection was assessed by indirect immunofluorescence labeling of the HA tag that was inserted in the corresponding Centauri construct followed by flow cytometry or confocal microscopy. Unless otherwise indicated, a threshold of 80% HA+ cells was set as a minimum value for performing αCentauri experiments.

Titration of αHIV Stocks and Infection. Virus yields were measured by p24 enzyme-linked immunosorbent assay according to the manufacturer's instructions (Clontech). MOIs were estimated by assuming that 1 ng of p24 corresponds to 5,000 transducing units (TU) (58). Viruses were treated with benzonase (Sigma, 15 min, 37 °C). Unless otherwise indicated, cells were infected at 2.5 TU per cell. Alternatively, viruses were titered by measuring Pol copy numbers by qPCR at 6 hpi in HeLa cells and infections were performed at given Pol copy numbers per cell. Unless otherwise stated, cells were infected at 2 Pol copies per cell.

Analysis of αCentauri^{GFP} Complementation. αCen^{GFP} reconstitution was assessed at 48 hpi by flow cytometry on fixed cells. Alternatively, cells were seeded in 96-well glass-bottomed Sensoplates (Greiner) at 10,000 cells per well at 24 hpi and acquired on a ThermoCellomics at 48 hpi after addition of live Hoechst 33342 (Molecular Probes).

Analysis of αCentauri^{NLuc} Complementation. CenNLS^{NLuc}-expressing cells, either transiently transduced or stable cell lines, were seeded in white opaque 96-well plates (Greiner) and infected the following day. αCen^{Nuc} reconstitution was assessed at 24 hpi by adding Nano-Glo substrate (Promega) according to the manufacturer's instructions. Other NLuc substrates were prepared by diluting the stock solution 1:50 in assay buffer (100 mM MES, pH 6.0, adjusted with KOH, 1 mM CDTA, 0.5% vol/vol Tergitol, 0.05% vol/vol antifoam, 150 mM KCl, 1 mM dithiothreitol, and 35 mM thiourea) and added to the cells 1:1. Luminescence was measured within 10 min using Tecan Infinite F200 Pro with 1,000 ms-integration and automatic attenuation.

β-Galactosidase and Bradford Assays. β-galactosidase assay was performed 48 hpi in indicator P4 cells according to the manufacturer's instructions (Roche Applied Science). Luciferase and β-galactosidase activities were normalized for protein concentration by the Bradford assay. Luminescence and absorbance were acquired on a Tecan Infinite F200 Pro.

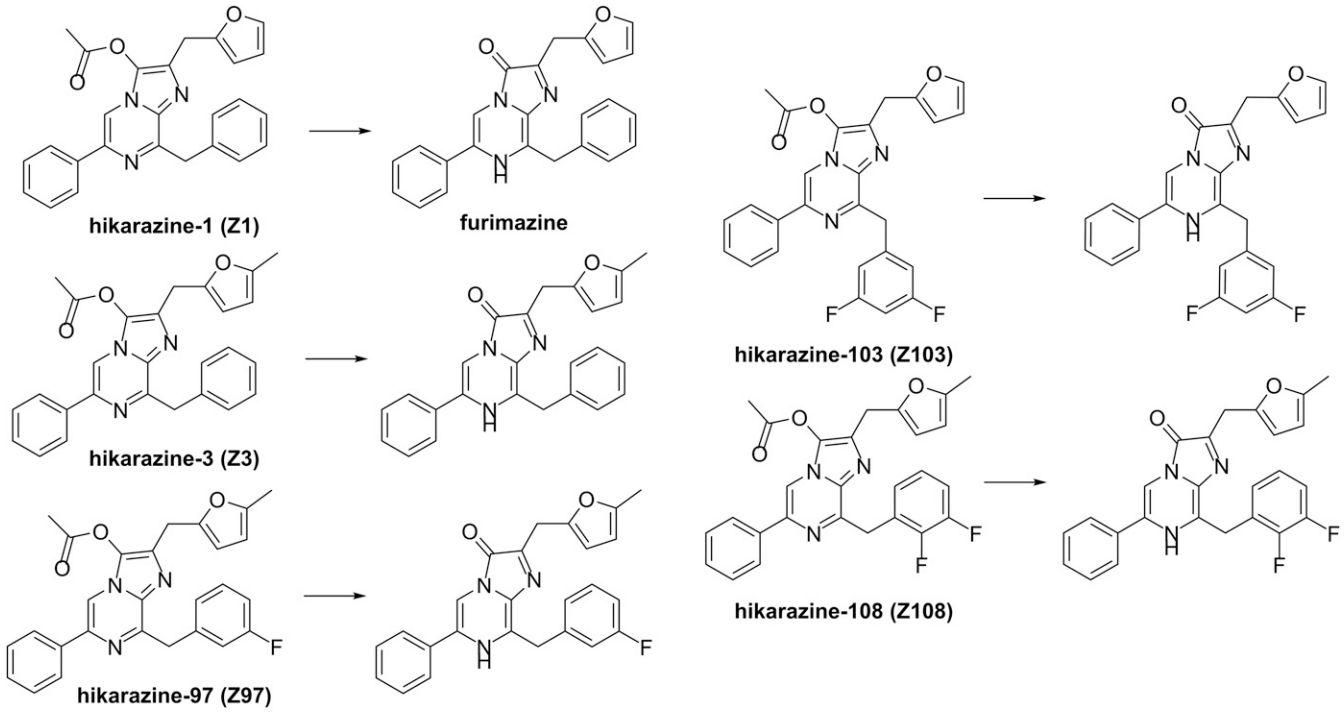

Scheme 2. Chemical formulae of the *O*-acetylated luciferins and luciferins used in the study.

qPCR. Total cellular DNA was isolated at 24 hpi using the QIAamp DNA micro kit (Qiagen). Two LTR (2-LTR)-containing circles were detected with primers MH535/536 and probe MH603 (59), using as the standard curve the pUC-2LTR plasmid, which contains the HIV-1 2-LTR junction. Reactions were normalized by amplification of the late reverse transcript with primers MH531/532 and probe LRT-P (59) or quantification of HIV-1 POL gene using specific primers as published previously (60). Alu-PCR was performed as published previously (32). Sequences of the different primers and probes are presented in Table 1.

Antibodies and Stains. The primary antibodies used were rat anti-HA tag (Roche 3F10) and mouse monoclonal anti-p24 clone AG3.0 and 183-H12-5C (NIH AIDS Reagent Program). Secondary antibodies were goat anti-mouse and anti-rabbit HRP conjugates (Thermo Fisher Scientific) or Alexa Fluor 455 or 647 conjugates. Intracellular Gag was measured using KC57 antibody conjugated to FITC or PE (Beckman Coulter).

Microscopy Immunolabeling and Imaging. Cultures were rinsed with phosphate-buffered saline (PBS) and fixed with 4% paraformaldehyde (electronic microscopy grade; Alfa Aesar) in PBS for 10 min at room temperature, treated with 50 mM NH_4Cl for 10 min, permeabilized with 0.5% Triton X-100 for 15 min, and blocked with 0.3% bovine serum albumin for 10 min. Cells were incubated with primary and secondary antibodies for 1 h and 30 min, respectively, in a moist chamber. Nuclei were labeled with Hoechst dye (Molecular Probes). Images were acquired using a LSM700 (Zeiss) confocal microscope equipped with a 63× objective or by Airyscan LSM800 (Zeiss), both operated by Zen software. Image analysis was performed using ImageJ.

Quality Controls. Z′ factors were calculated using 10 to 30 replicates per condition, randomly distributed on the plate. The Z-factor (61) is a measure that quantifies the separation between the distribution of positive and negative controls:

$$\text{Z-factor} = 1 - \frac{3(\sigma_p + \sigma_n)}{\left|\mu_p - \mu_n\right|},$$

where μ_p and σ_p are the mean and SD values of the positive control and μ_n and σ_n are those of the negative control.

If robust, the Z-factor is calculated using robust estimates of location (median) and spread (mad).

The signal/background ($\mu_p - \mu_n$) and signal/noise ($(\mu_p - \mu_n)/\sigma_n$) ratios are also provided.

All statistical analysis was performed with R programming language (62).

Generation of Luciferin Solutions from the *O*-Acetylated Luciferins. The considered *O*-acetylated luciferin (1 mg) was dissolved in dimethyl sulfoxide (DMSO) (0.2 mL) and then diluted by adding a solution of acidic ethanol (0.3 mL) made from the addition of 37% hydrochloric acid (100 μL) on 100% ethanol (12 mL). The 0.5-mL reaction solution was incubated at 50 °C for 2 h to give a luciferin stock solution which was aliquoted and frozen at −80 °C for later use (Scheme 1). The *O*-acetylated luciferins (hikarazines) and the corresponding luciferins used in this work are depicted in Scheme 2.

RNA Interference. LV coding for shRNA against Pin1, CypA, RanBP2, TNPO1, TNPO3, CKAP1, WIRE, MAP1A, MAP1S, IPO5, IPO7, and KPNB1 were generated as previously published (31, 32, 35, 63, 64). Transduction was performed at MOI 50.

Statistical Analyses. Unpaired and paired *t* tests, ordinary one-way ANOVA, and R^2 coefficients were obtained using Prism 6.

Data Availability. The authors make all data available upon request.

ACKNOWLEDGMENTS. This work was financed by Sidaction, the Société d'Accélération de Transfert Technologique IdfInnov (now Erganeo), the Labex EpiGenMed "Investissements d'avenir" ANR-10-LABX-12-01, the ATIP-Avenir program, and the Agence Nationale de Recherche sur le Sida et les Hépatites Virales. We thank Leslie Bancel-Vallee (Montpellier Ressources Imagerie, Montpellier) for help with the Airyscan imaging.

1. J. G. Park *et al*., Identification and characterization of novel compounds with broad-spectrum antiviral activity against influenza A and B viruses. *J. Virol.* **94**, e02149-19 (2020).
2. F. Touret *et al*., In vitro screening of a FDA approved chemical library reveals potential inhibitors of SARS-CoV-2 replication. bioRxiv:10.1101/2020.04.03.023846 (5 April 2020).
3. L. M. Johansen *et al*., FDA-approved selective estrogen receptor modulators inhibit Ebola virus infection. *Sci. Transl. Med.* **5**, 190ra79 (2013).
4. M. A. Rameix-Welti *et al*., Visualizing the replication of respiratory syncytial virus in cells and in living mice. *Nat. Commun.* **5**, 5104 (2014).
5. R. König *et al*., Human host factors required for influenza virus replication. *Nature* **463**, 813–817 (2010).
6. T. Inoue, B. Tsai, How viruses use the endoplasmic reticulum for entry, replication, and assembly. *Cold Spring Harb. Perspect. Biol.* **5**, a013250 (2013).
7. S. Cohen, S. Au, N. Panté, How viruses access the nucleus. *Biochim. Biophys. Acta* **1813**, 1634–1645 (2011).
8. J. D. Pédelacq, S. Cabantous, T. Tran, T. C. Terwilliger, G. S. Waldo, Engineering and characterization of a superfolder green fluorescent protein. *Nat. Biotechnol.* **24**, 79–88 (2006).
9. M. P. Hall *et al*., Engineered luciferase reporter from a deep sea shrimp utilizing a novel imidazopyrazinone substrate. *ACS Chem. Biol.* **7**, 1848–1857 (2012).
10. Y. Suzuki, R. Craigie, The road to chromatin - nuclear entry of retroviruses. *Nat. Rev. Microbiol.* **5**, 187–196 (2007).
11. K. A. Matreyek, A. Engelman, Viral and cellular requirements for the nuclear entry of retroviral preintegration nucleoprotein complexes. *Viruses* **5**, 2483–2511 (2013).
12. A. Dharan, N. Bachmann, S. Talley, V. Zwikelmaier, E. M. Campbell, Nuclear pore blockade reveals that HIV-1 completes reverse transcription and uncoating in the nucleus. *Nat. Microbiol.* **5**, 1088–1095 (2020).
13. R. C. Burdick *et al*., HIV-1 uncoats in the nucleus near sites of integration. *Proc. Natl. Acad. Sci. U.S.A.* **117**, 5486–5493 (2020).
14. S. Cabantous, T. C. Terwilliger, G. S. Waldo, Protein tagging and detection with engineered self-assembling fragments of green fluorescent protein. *Nat. Biotechnol.* **23**, 102–107 (2005).
15. A. S. Dixon *et al*., NanoLuc complementation reporter optimized for accurate measurement of protein interactions in cells. *ACS Chem. Biol.* **11**, 400–408 (2016).
16. T. Jacks *et al*., Characterization of ribosomal frameshifting in HIV-1 gag-pol expression. *Nature* **331**, 280–283 (1988).
17. A. N. Engelman, P. Cherepanov, Retroviral intasomes arising. *Curr. Opin. Struct. Biol.* **47**, 23–29 (2017).
18. L. C. Mulder, M. A. Muesing, Degradation of HIV-1 integrase by the N-end rule pathway. *J. Biol. Chem.* **275**, 29749–29753 (2000).
19. E. Devroe, A. Engelman, P. A. Silver, Intracellular transport of human immunodeficiency virus type 1 integrase. *J. Cell Sci.* **116**, 4401–4408 (2003).
20. N. J. Arhel *et al*., HIV-1 DNA Flap formation promotes uncoating of the pre-integration complex at the nuclear pore. *EMBO J.* **26**, 3025–3037 (2007).
21. A. E. Hulme, O. Perez, T. J. Hope, Complementary assays reveal a relationship between HIV-1 uncoating and reverse transcription. *Proc. Natl. Acad. Sci. U.S.A.* **108**, 9975–9980 (2011).
22. Y. Yang, T. Fricke, F. Diaz-Griffero, Inhibition of reverse transcriptase activity increases stability of the HIV-1 core. *J. Virol.* **87**, 683–687 (2013).
23. V. Zennou *et al*., HIV-1 genome nuclear import is mediated by a central DNA flap. *Cell* **101**, 173–185 (2000).
24. C. D. Hu, T. K. Kerppola, Simultaneous visualization of multiple protein interactions in living cells using multicolor fluorescence complementation analysis. *Nat. Biotechnol.* **21**, 539–545 (2003).
25. M. S. Stake, D. V. Bann, R. J. Kaddis, L. J. Parent, Nuclear trafficking of retroviral RNAs and Gag proteins during late steps of replication. *Viruses* **5**, 2767–2795 (2013).
26. A. L. Brass *et al*., Identification of host proteins required for HIV infection through a functional genomic screen. *Science* **319**, 921–926 (2008).
27. R. König *et al*., Global analysis of host-pathogen interactions that regulate early-stage HIV-1 replication. *Cell* **135**, 49–60 (2008).
28. Y. Tomabechi *et al*., Crystal structure of nanoKAZ: The mutated 19 kDa component of Oplophorus luciferase catalyzing the bioluminescent reaction with coelenterazine. *Biochem. Biophys. Res. Commun.* **470**, 88–93 (2016).
29. E. P. Coutant *et al*., Gram-scale synthesis of luciferins derived from coelenterazine and original insights into their bioluminescence properties. *Org. Biomol. Chem.* **17**, 3709–3713 (2019).
30. E. P. Coutant *et al*., Bioluminescence profiling of NanoKAZ/NanoLuc luciferase using a chemical library of coelenterazine analogues. *Chemistry* **26**, 948–958 (2020).
31. J. Fernandez *et al*., Microtubule-associated proteins 1 (MAP1) promote human immunodeficiency virus type I (HIV-1) intracytoplasmic routing to the nucleus. *J. Biol. Chem.* **290**, 4631–4646 (2015).
32. F. Di Nunzio *et al*., Human nucleoporins promote HIV-1 docking at the nuclear pore, nuclear import and integration. *PLoS One* **7**, e46037 (2012).
33. T. Schaller *et al*., HIV-1 capsid-cyclophilin interactions determine nuclear import pathway, integration targeting and replication efficiency. *PLoS Pathog.* **7**, e1002439 (2011).
34. R. Zhang, R. Mehla, A. Chauhan, Perturbation of host nuclear membrane component RanBP2 impairs the nuclear import of human immunodeficiency virus -1 preintegration complex (DNA). *PLoS One* **5**, e15620 (2010).
35. J. Fernandez *et al*., Transportin-1 binds to the HIV-1 capsid via a nuclear localization signal and triggers uncoating. *Nat. Microbiol.* **4**, 1840–1850 (2019).
36. A. De Iaco *et al*., TNPO3 protects HIV-1 replication from CPSF6-mediated capsid stabilization in the host cell cytoplasm. *Retrovirology* **10**, 20 (2013).

37. T. Fricke *et al*., The ability of TNPO3-depleted cells to inhibit HIV-1 infection requires CPSF6. *Retrovirology* **10**, 46 (2013).
38. S. Matsuoka, E. Dam, D. Lecossier, F. Clavel, A. J. Hance, Modulation of HIV-1 infectivity and cyclophilin A-dependence by Gag sequence and target cell type. *Retrovirology* **6**, 21 (2009).
39. A. De Iaco, J. Luban, Cyclophilin A promotes HIV-1 reverse transcription but its effect on transduction correlates best with its effect on nuclear entry of viral cDNA. *Retrovirology* **11**, 11 (2014).
40. R. Truant, B. R. Cullen, The arginine-rich domains present in human immunodeficiency virus type 1 Tat and Rev function as direct importin beta-dependent nuclear localization signals. *Mol. Cell. Biol.* **19**, 1210–1217 (1999).
41. S. Misumi *et al*., Uncoating of human immunodeficiency virus type 1 requires prolyl isomerase Pin1. *J. Biol. Chem.* **285**, 25185–25195 (2010).
42. M. Kane *et al*., Nuclear pore heterogeneity influences HIV-1 infection and the antiviral activity of MX2. *eLife* **7**, e35738 (2018).
43. M. D. J. Dicks *et al*., Multiple components of the nuclear pore complex interact with the amino-terminus of MX2 to facilitate HIV-1 restriction. *PLoS Pathog.* **14**, e1007408 (2018).
44. A. De Iaco, J. Luban, Inhibition of HIV-1 infection by TNPO3 depletion is determined by capsid and detectable after viral cDNA enters the nucleus. *Retrovirology* **8**, 98 (2011).
45. J. C. Valle-Casuso *et al*., TNPO3 is required for HIV-1 replication after nuclear import but prior to integration and binds the HIV-1 core. *J. Virol.* **86**, 5931–5936 (2012).
46. A. Cribier *et al*., Mutations affecting interaction of integrase with TNPO3 do not prevent HIV-1 cDNA nuclear import. *Retrovirology* **8**, 104 (2011).
47. M. J. Basse *et al*., 2P2Idb: A structural database dedicated to orthosteric modulation of protein-protein interactions. *Nucleic Acids Res.* **41**, D824–D827 (2013).
48. M. Cavrois, C. De Noronha, W. C. Greene, A sensitive and specific enzyme-based assay detecting HIV-1 virion fusion in primary T lymphocytes. *Nat. Biotechnol.* **20**, 1151–1154 (2002).
49. C. Burkard *et al*., Dissecting virus entry: Replication-independent analysis of virus binding, internalization, and penetration using minimal complementation of β-galactosidase. *PLoS One* **9**, e101762 (2014).
50. S. V. Avilov *et al*., Replication-competent influenza A virus that encodes a split-green fluorescent protein-tagged PB2 polymerase subunit allows live-cell imaging of the virus life cycle. *J. Virol.* **86**, 1433–1448 (2012).
51. C. R. Chin *et al*., Direct visualization of HIV-1 replication intermediates shows that capsid and CPSF6 modulate HIV-1 intra-nuclear invasion and integration. *Cell Rep.* **13**, 1717–1731 (2015).
52. R. C. Burdick, W. S. Hu, V. K. Pathak, Nuclear import of APOBEC3F-labeled HIV-1 preintegration complexes. *Proc. Natl. Acad. Sci. U.S.A.* **110**, E4780–E4789 (2013).
53. C. Di Primio *et al*., Single-cell imaging of HIV-1 provirus (SCIP). *Proc. Natl. Acad. Sci. U.S.A.* **110**, 5636–5641 (2013).
54. D. Mandal, V. R. Prasad, Analysis of 2-LTR circle junctions of viral DNA in infected cells. *Methods Mol. Biol.* **485**, 73–85 (2009).
55. C. M. Farnet, W. A. Haseltine, Circularization of human immunodeficiency virus type 1 DNA in vitro. *J. Virol.* **65**, 6942–6952 (1991).
56. S. Thierry *et al*., Integrase inhibitor reversal dynamics indicate unintegrated HIV-1 dna initiate de novo integration. *Retrovirology* **12**, 24 (2015).
57. A. Amara *et al*., G protein-dependent CCR5 signaling is not required for efficient infection of primary T lymphocytes and macrophages by R5 human immunodeficiency virus type 1 isolates. *J. Virol.* **77**, 2550–2558 (2003).
58. R. Zufferey *et al*., Self-inactivating lentivirus vector for safe and efficient in vivo gene delivery. *J. Virol.* **72**, 9873–9880 (1998).
59. S. L. Butler, M. S. Hansen, F. D. Bushman, A quantitative assay for HIV DNA integration in vivo. *Nat. Med.* **7**, 631–634 (2001).
60. C. Iglesias *et al*., Residual HIV-1 DNA Flap-independent nuclear import of cPPT/CTS double mutant viruses does not support spreading infection. *Retrovirology* **8**, 92 (2011).
61. J. H. Zhang, T. D. Chung, K. R. Oldenburg, A simple statistical parameter for use in evaluation and validation of high throughput screening assays. *J. Biomol. Screen.* **4**, 67–73 (1999).
62. R. C. Team, *A Language and Environment for Statistical Computing* (R Foundation for Statistical Computing, Vienna, 2019).
63. G. Maarifi *et al*., TRIM8 is required for virus-induced IFN response in human plasmacytoid dendritic cells. *Sci. Adv.* **5**, eaax3511 (2019).
64. A. Kaul *et al*., Essential role of cyclophilin A for hepatitis C virus replication and virus production and possible link to polyprotein cleavage kinetics. *PLoS Pathog.* **5**, e1000546 (2009).